Cohesive Fracturing and Stresses Caused by Hydration Heat in Massive Concrete Wall

Zdeněk P. Bažant, F.ASCE[1]; Jin-Keun Kim[2]; and Sang-Eun Jeon[3]

Abstract: Avoidance of cracking damage due to hydration is an important objective in the design of nuclear reactor containments. Assessment of the safety against cracking requires a realistic material model and its effective numerical implementation. Toward this goal, the paper develops a comprehensive material model which includes approximate simulation of cracking based on the principles of cohesive fracture mechanics, as well as an up-to-date creep formulation with aging and temperature effects. A standard heat conduction model is incorporated in the analysis as well. Since the crack width is the most important characteristic of cracking damage, particular attention is paid to crack spacing which governs crack width. The results of stability analysis of parallel crack systems based on fracture mechanics are used to estimate the spacing of open cracks as a function of their depth. Numerical simulations clarifying various aspects of hydration heat effects are presented.

DOI: 10.1061/(ASCE)0733-9399(2003)129:1(21)

CE Database keywords: Walls; Concrete; Cracking; Stress; Simulation.

Introduction

Thermal stresses due to hydration heat can cause extensive cracking in massive concrete structures. To avoid it, the design must be based on realistic calculations.

The problem of high temperature effects on concrete (Bertero and Polivka 1972; Bernander and Gustafsson 1981; Emborg 1985; Bažant and Kaplan 1996; etc.), and specifically the problem of cracking due to hydration heat, have been studied continuously since the building of large dams began in the 1930s (e.g., Lea and Jones 1935; Carlson and Forbrick 1938) (see also Maslov 1940; Czernin 1962; Lea 1970; Neville 1981). Because of the current heightened concern with the safety of nuclear power plants, the problem has recently received renewed attention aimed at designing nuclear containments and their construction procedure. More relalistic predictions of the width of cracks caused by hydration heat are needed to adopt proper mitigating measures (such as cooling of concrete mix, cooling of the wall after casting, choice of cement type and admixtures, the amount, size and layout of reinforcement, the level of prestress, etc.).

Since fracture mechanics of quasibrittle materials such as concrete (Bažant and Planas 1998) is a relatively young theory, it is not surprising that, despite the long history of research, its role has not been investigated nor appreciated in the design community. The energetic aspects of crack propagation are the dominant consideration in determining the spacing of thermal cracks. The spacing of cracks governs their opening width, which is of main concern in design. The width in turn governs the stiffness of cracked concrete and thereby affects the magnitude of thermal stresses.

The purpose of this paper is to present a comprehensive mathematical model for determining the stresses and the width of the cracks produced by hydration heat in a massive concrete wall such as the wall of a nuclear containment shell. The considerations of crack spacing will be embedded in the classical smeared cracking concept. Aside from an algorithm for the opening and closing of cracks, the model will incorporate up-to-date algorithms for creep of young concrete and its aging at variable temperature. The evolution of temperature distributions will be included in the numerical calculations, and the effect of temperature-dependent aging on the rate of generation of hydration heat will be taken into account.

The modeling will exploit several simplifying features of the problem of hydration heat in a thick wall. While the gradient of temperature causes the pore water in concrete to diffuse in the direction of decreasing temperature, in a massive wall the water diffusion is a very slow process lasting many years. It cannot be significant during the relatively short period of elevated temperature caused by hydration (lasting only a few weeks), and will therefore be neglected. Although diffusion of pore water is also caused by drying from the surface, this effect, too, can be neglected—not only for the reason just mentioned but also because, during the period of elevated temperatures due to hydration, the surface of concrete is normally protected from drying.

Furthermore, since only the central part of a far-extending wall will be considered, the initial normals to the wall may be assumed to remain straight and normal, the strains ϵ_y and ϵ_z in the in-plane coordinate directions y and z (Fig. 1) to remain uniform, and the problem to be spatially one dimensional in transverse direction x. This will be another helpful simplification. Since the curvature

[1]McCormick School Professor and W. P. Murphy Professor of Civil Engineering and Materials Science, Northwestern Univ., 2145 Sheridan Rd., Evanston, IL 60208 (corresponding author). E-mail: z-bazant@northwestern.edu.

[2]Professor, Dept. of Civil Engineering, Korea Advanced Institute of Science and Technology, 373-1 Kusong, Yusong, Taejon 305-701, Korea.

[3]Student, Dept. of Civil Engineering, Korea Advanced Institute of Science and Technology, 373-1 Kusong, Yusong, Taejon 305-701, Korea.

Note. Associate Editor: Franz-Josef Ulm. Discussion open until June 1, 2003. Separate discussions must be submitted for individual papers. To extend the closing date by one month, a written request must be filed with the ASCE Managing Editor. The manuscript for this paper was submitted for review and possible publication on October 3, 2001; approved on May 3, 2002. This paper is part of the ***Journal of Engineering Mechanics***, Vol. 129, No. 1, January 1, 2003. ©ASCE, ISSN 0733-9399/2003/1-21–30/$18.00.

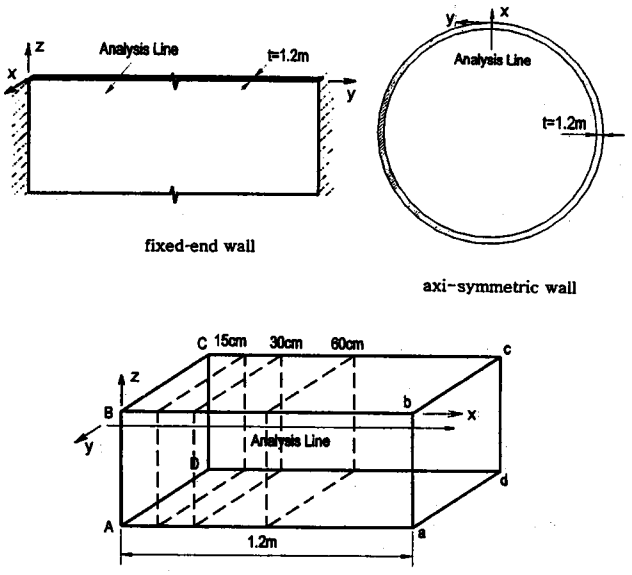

Fig. 1. Element of planar wall fixed at ends (top left), and cylindrical wall (top right), both analyzed one dimensionally, and wall element considered in numerical analysis (bottom)

radius of the wall is large compared to the thickness of the wall, the curvature will be neglected.

The effect of reinforcement will be neglected in the present analysis, although the way to consider it is well known and not very difficult. Since the main effect of reinforcement is to reduce the spacing, and thus the width, of tensile cracks (Bažant and Wahab 1980), the neglect of reinforcement leads to the worst possible prediction and is on the side of safety.

Evolution of Temperature Distributions

The heat flux q in the direction of coordinate x and the heat balance condition may be written as

$$q=-b\frac{\partial T}{\partial x},\quad \rho C\frac{\partial T}{\partial t}=-\frac{\partial q}{\partial x}+\rho_c\dot{H}(t_e) \tag{1}$$

(e.g., Bažant and Kaplan 1996, p. 201); here t = time (measured from the instant of set of concrete); T = absolute temperature; b = heat conductivity of (wet) concrete (typically 2.3 W/m°C) (Bažant and Kaplan 1996, p. 65), whose temperature dependence (Neville 1981) is only mild and is here neglected; ρ = mass density of concrete; C = isobaric heat capacity (specific heat) of (wet) concrete (typically $C\approx$ 1,100 J/(kg°C, but it ranges from 840 to 1,170, according to Neville 1981, p. 491; or Bažant and Kaplan 1996, pp. 60 and 212); and ρ_c = mass of cement per unit volume of concrete. Furthermore, $\dot{H}(t_e)$ = rate of heat generation (per unit mass of cement) by the exothermal chemical reactions of hydration. This rate is considered to be a given function of the degree of hydration, which may be characterized by the equivalent hydration period t_e (also called the maturity)

$$t_e(x,t)=\int_0^t \beta_T(x,t')\,dt'$$
$$\beta_T(x,t')=\exp\left[\frac{U}{R}\left(\frac{1}{T_0}-\frac{1}{T(x,t')}\right)\right] \tag{2}$$

Here U = effective activation energy of cement hydration (which characterizes the rate of heat generation); R = universal gas constant; and T_0 = reference temperature; usually $T_0=273+25$ K. In the absence of tests, the function $\dot{H}(T,t_e)$ may be approximately estimated from the data presented in Bažant and Kaplan (1996) or Neville (1981, p. 42, Fig. 1.16).

Substituting the first of Eq. (1) into the second, we get

$$\rho C\frac{\partial T}{\partial t}=b\frac{\partial^2 T}{\partial x^2}+\rho_c\dot{H}(t_e) \tag{3}$$

This is the one-dimensional diffusion equation for heat conduction with a distributed heat source $\rho_c\dot{H}$. The dependence of heat conductivity of concrete on its temperature and degree of hydration (as well as moisture content) is here neglected as it is rather weak. Also neglected is the effect of cracking on heat conductivity.

The initial condition at $t=0$ (the moment of set of concrete) and all x is $T=T_1$ = given initial temperature, considered to be uniform. The concrete wall is considered to occupy the region $-h/2\leqslant x\leqslant h/2$ (Fig. 1). Since the thickness h_f of the formwork (or any cover that may provide thermal insulation) is small compared to the wall thickness ($h_f\ll h$), the temperature distribution across the formwork is almost linear for most of the time, and so the thermal boundary conditions may be written as

$$b\frac{\partial T}{\partial x}=\pm b_f\frac{T-T_e}{h_f}\quad \text{for } x=\mp\frac{h}{2},\quad t\geqslant 0 \tag{4}$$

where b_f = heat conductivity of the formwork. The temperature T_s at the surface of the formwork is not exactly the same as the environmental temperature T_e, and the proper boundary condition at the surface of the formwork is $q=\mu_s(T_e-T_s)$, where μ_s = surface emissivity, which depends mainly of the circulation of air. This may be conveniently taken into account by imagining a layer of thickness h_f^{ad} (called the equivalent surface thickness) to be added to the formwork. Considering a linear temperature distribution across the formwork, an added layer of thickness $h_f^{\text{ad}}=b_f/\mu_s$ gives the same heat flux as a finite surface emissivity. Thus the aforementioned boundary conditions Eq. (4) remain valid if we assume the formwork thickness in the calculations to represent the actual formwork thickness increased by h_f^{ad}. For approximate calculations, though, we may assume $h_f^{\text{ad}}\approx 0$.

To justify our neglect of moisture transport, let us compare the rates of the heating and drying processes. The heat diffusivity is $D_T=b/(\rho C)$, and for the aforementioned values (with $\rho=2300$ kg/m^3 and 1 calorie = 4.1868 J) one gets the typical estimate $D_T=0.41$ cm^2/s. It is illuminating to compare this to the diffusivity of pore water, which is typically $D_w=0.1$ cm^2/day for mature concrete (Bažant and Najjar 1972), and roughly 10× larger for concrete 1 week old. The characteristic time for drying, which may be taken as the time for a front of drying to penetrate from the outer face to the middle of the wall of a typical reactor containment, is about

$$t_{\text{ch}w}=(h/2)^2/12D_w=4.6\ \text{years} \tag{5}$$

where h = wall thickness, here considered as $h=0.9$ m. This should be compared with the characteristic time for heat conduction in the wall of the same thickness, which is taken as the time for a heat front to propagate from a heated face to the middle of the wall

$$t_{\text{ch}T}=(h/2)^2/12D_T=6.9\ \text{min}\ll t_{\text{ch}w} \tag{6}$$

Because of continued heating by hydration, elevated temperatures

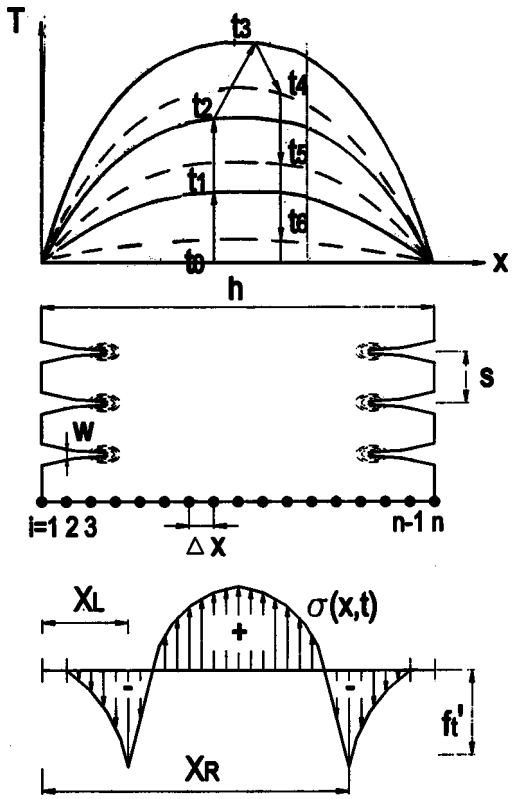

Fig. 2. (Top) Sequence of temperature profiles at subsequent times $t_0, t_1, \ldots, t_6$ during hydration. (Middle) Parallel thermal cracks (opening grossly exaggerated) and nodal subdivision. (Bottom) Typical stress distribution after formation of cohesive cracks.

may persist in the wall for several weeks. Since 6.9 min, as well as the period of several weeks is much less than 4.6 years, we are justified in neglecting the effect of moisture diffusion. However, for much thicker bodies such as gravity dams, in which the elevated temperatures persist far longer, moisture diffusion becomes important (one might wonder whether cracking could accelerate overall moisture diffusion enough to influence the heating of containment wall; however, this acceleration is less than 1 order of magnitude for normal crack width) (see Bažant et al. 1987).

Numerical Solution of Temperature Distributions

The conductivity b and heat capacity C of concrete may be taken approximately as constant. If $\dot{H}$ too were a constant, the diffusion equation (3) would be linear. The solution for a wall, having the form of Fourier series, could then be taken directly from Carslaw and Jaeger's book (Carslaw and Jaeger 1959). However, $\dot{H}$ depends on the temperature history, which makes the problem nonlinear (Bažant and Kaplan 1996).

There are two ways to solve the evolutions of temperature profiles $T(x,t)$ (Fig. 2 top) from the nonlinear diffusion equation: (1) solve Eq. (3) by finite differences, or (2) substitute the unknown temperature-dependent heat generation $\dot{H}$ into the Fourier series solution and use the Levenberg–Marquardt nonlinear optimization algorithm. In the latter, in order to achieve convergence, one would need to set $\dot{H}(t_e)=H_\infty g(t_e)$, where $g(t_e)=$given function and $H_\infty=$total heat liberated upon reaching the maximum possible degree of hydration of cement (not all the cement present in concrete can be hydrated). The value of H_∞ may be gradually increased in small steps up to the correct value and, for each value of H_∞, optimization may be conducted using the solution for the previous value of H_∞ as the initial estimate.

We pursue the former. We subdivide the cross-wall coordinate x by n nodal points x_i $(i=1,2,...n)$ into $n-1$ equal intervals (or elements) Δx (Fig. 1), and the time t by discrete times t_r $(r=1,2,...N)$ into N time steps $\Delta t=t_{r+1}-t_r$. The time steps should be increased with time, for the sake of computational efficiency. We use a Crank–Nicolson type algorithm (Crank 1957), which is based on central difference approximations for the spatial and temporal derivatives in Eq. (3), centered at x_i and at $(t_r+t_{r+1})/2$;

$$\frac{b}{2\Delta x^2}(T_{i-1,r+1}-2T_{i,r+1}+T_{i+1,r+1}+T_{i-1,r}-2T_{i,r}+T_{i+1,r}) = \frac{\rho C}{\Delta t}(T_{i,r+1}-T_{i,r})-\frac{\rho_c}{2}(\dot{H}_{i,r+1}+\dot{H}_{i,r}) \tag{7}$$

The values of temperature T at t_{r+1} are the unknowns. Isolating them on the left-hand side, we get the following system of difference equations:

$$\frac{b}{2\Delta x^2}(T_{i-1,r+1}+T_{i+1,r+1})-\left(\frac{\rho C}{\Delta t}+\frac{b}{\Delta x^2}\right)T_{i,r+1} = -\frac{\rho_c}{2}[\dot{H}(T_{i,r+1},t_{e_{i,r+1}})+\dot{H}(T_{i,r},t_{e_{i,r}})] -\left(\frac{\rho C}{\Delta t}-\frac{b}{\Delta x^2}\right)T_{i,r}-\frac{b}{2\Delta x^2}(T_{i+1,r}+T_{i-1,r}) \tag{8}$$

$(i=2,3,...,n-1)$. This represents a banded system of $n-2$ equations for $n-2$ unknowns $T_{2,r+1}$, $T_{3,r+1},\ldots,T_{n-1,r+1}$. The values of $T_{1,r+1}$ and $T_{n,r+1}$ are known from the boundary condition.

If the values of T at the surface nodes are not specified, then $T_{1,r+1}$, $T_{n,r+1}$ become two additional unknowns and one needs to add to the equation system the more general boundary conditions in Eq. (4). Their discrete form is

$$\frac{b}{\Delta x}(T_{2,r+1}-T_{1,r+1})=\frac{b_f}{h_f}(T_{1,r+1}-T_e)$$
$$\frac{b}{\Delta x}(T_{n-1,r+1}-T_{n,r+1})=\frac{b_f}{h_f}(T_{n,r+1}-T_e) \tag{9}$$

The case of a perfectly insulated surface can be modeled most simply (while retaining second-order accuracy) if one lets the boundary element straddle the surface (the actual surface being located in the middle of the element) and assumes for that element a zero heat conductivity $b_f=0$. This is also the simplest way to handle the condition of symmetry at the midthickness of the wall $x=0$.

The discrete values of the equivalent hydration period t_e are calculated, according to Eq. (2), from the incremental relation

$$t_{e_{i,r+1}}=t_{ei,r}+\Delta t\exp\left[\frac{U}{R}\left(\frac{1}{T_0}-\frac{2}{T_{i,r}+T_{i,r+1}}\right)\right] \tag{10}$$

Because $\dot{H}_{i,r+1}$ depends on the unknown $T_{i,r+1}$ through $t_{e_{i,r+1}}$, and possibly also directly, Eq. (8) represents nonlinear equations. Therefore, iteration of the time step is needed. In each iteration,

$t_{e_{i,r+1}}$ and $\dot{H}(T_{i,r+1}, t_{e_{i,r+1}})$ are evaluated using the $T_{i,r+1}$ value from the preceding iteration. But for the first analysis of the time step, they are evaluated from the preceding time step.

Aging Viscoelastic Behavior

Let us assume that, during the heating of concrete by hydration, the resultant forces in the cross section of a wall (Fig. 1), per unit distances in the y and z directions, include only the normal force N_y, which is given, while the bending moments $M_y = M_z = 0$. For the sake of simplicity, we further assume that, at every x, the normal forces in the in-plane directions y and z are the same, $N_z = N_y$, [i.e., that the stress state is everywhere biaxial (in reality, N_z and N_y may of course be quite different, but our main objective is to illustrate the solution procedure, which would be similar even if $N_z \neq N_y$)]. Restricting attention to the central portion of a far extending wall of uniform properties, the in-plane normal strain ϵ in the wall, caused by hydration heat, must be uniform throughout the wall thickness h and the same in both y and z directions; $\epsilon_y = \epsilon_z = \epsilon$. The in-plane normal stresses σ at the same x are also the same in both y and z directions but of course vary with x throughout the wall thickness.

Furthermore, since there are no shear forces, we may consider the thermal cracks emanating from the surfaces to be normal to the wall. It will not be an excessive simplification if we assume these cracks to be normal to either y or z axes. For the purpose of one-dimensional analysis, we imagine these cracks to be continuously smeared. Accordingly, despite crack formation, all the cross sections (or all the normals to the wall, at any location y,z) may be considered to be in the same state, and $\sigma_{xy} = \sigma_{xz} = \sigma_{yz} = \sigma_x = 0$. These assumptions render one-dimensional analysis possible.

Let ξ be the cracking (or fracturing) normal strains in the y and z directions. The strain in the concrete between the cracks, which is $\epsilon - \xi$, must follow the viscoelastic constitutive equation for uncracked concrete, with the aging of course included. The elastic strains and creep at variable stress may be determined by applying the principle of superposition for concrete creep (see, e.g., Bažant 1982; RILEM 1988). This leads to the following biaxial constitutive relation with aging:

$$\epsilon(t) - \xi(t) = \int_0^t J^b(t,t')\sigma(x,\mathrm{d}t') + \alpha[T(x,t) - T_0] \qquad (11)$$

(Bažant and Chern 1985a); here $t = 0$ corresponds to the instant of the set of concrete (i.e., the moment when concrete ceases being a liquid); α = thermal expansion coefficient of concrete (which is about 10^{-5}); $J^b(t,t') = (1-\nu)J(t,t')$ = biaxial compliance function of concrete, representing the strain at age t caused by a unit biaxial stress applied at age t'; ν = Poisson ratio of concrete ($\nu \approx$ constant = 0.18 for both elastic strains and creep); $J(t,t')$ = uniaxial compliance function of concrete, on which extensive test data are available (e.g., Hanson 1953; Harboe 1958; RILEM 1988; Bažant and Baweja 2000; Jirásek and Bažant 2002). The notation $\sigma(x,\mathrm{d}t')$ defines the so-called Stieltjes integral, which has the advantage that it is defined not only for continuous stress histories but also for discontinuous histories which stress jumps. In time intervals with a continuous stress variation, the Stieltjes integral may be reduced to the standard (Riemann) integral by setting:

$$\sigma(x,\mathrm{d}t') = \frac{\partial \sigma(x,t')}{\partial t'}\,\mathrm{d}t' \qquad (12)$$

For computations, it would be more efficient to replace the integral-type constitutive relation in Eq. (11) with an equivalent rate-type constitutive relation based on the Kelvin or Maxwell chain and the solidification theory (e.g., RILEM 1988; Bažant 1995; Jirásek and Bažant 2001). We do not need to pursue it, however, because computational efficiency is not important in a one-dimensional problem (multidimensional generalizations would of course be a different matter).

A realistic long-time compliance function (Bažant and Prasannan 1989; Bažant 1995, Bažant and Baweja 2000) for concrete can be defined by a simple expression for the compliance rate $\dot{J}$, but a simple, exactly equivalent, expression for $J(t,t')$ does not exist (because, due to aging, the integration leads to a general binomial integral which cannot be integrated in a closed form). For a numerical step-by-step solution, however, an expression for the total compliance J is not needed. It suffices, and is actually simpler, to use an expression for the compliance rate $\dot{J}(t,t') = \partial J(t,t')/\partial t$. Therefore, we differentiate Eq. (11) with respect to t and multiply the resulting expression by the time increment $\Delta t = t_{r+1} - t_r$. Thus we obtain for the strain increment $\Delta\epsilon = \epsilon_{r+1} - \epsilon_r$ the following central difference approximation:

$$\Delta\epsilon = C_v \Delta\sigma_i + \Delta\epsilon_i^v + \alpha\Delta T_i + \Delta\xi_i \qquad (13)$$

$$C_v = J^b_{r+1,r}$$
$$\Delta\epsilon_i^v = \Delta t \sum_{q=1}^{r-1} \dot{J}^b_{r+1,q+(1/2)}(\sigma_{i,q+1} - \sigma_{i,q}) \qquad (14)$$

(Bažant 1982; Bažant and Kaplan 1996; Jirásek and Bažant 2002) where we dropped subscript i from $\Delta\epsilon$ because, according to our assumptions, the stress profiles in the wall are symmetric and the strain ϵ may be considered to be constant throughout the wall thickness; we also introduced the short notation $J^b_{r,q} = J^b(t_r, t_q)$; $\Delta\epsilon_i^v$ = viscoelasic strain increment; C_v represents the biaxial short-time viscoelastic compliance for the current time step; subscript $q + \frac{1}{2}$ refers to the value at time $(t_q + t_{q+1})/2$ (which can be approximated as the average of the J^b values at t_q and t_{q+1}); i.e., $\dot{J}^b_{r+1,q+(1/2)} = (\dot{J}^b_{r+1,q} + \dot{J}^b_{r+1,q+1})/2$. Furthermore, one might wonder whether $C_v = J^b_{r+1,r+(1/2)}$ would not be a better approximation, but the approximation in Eq. (14), which corresponds to the effective modulus for creep, is actually more accurate (RILEM 1988).

Equilibrium in the cross section of the wall requires that

$$\int_0^h \sigma(x,t)\,\mathrm{d}x = N_y(t) \quad (t \geq 0) \qquad (15)$$

For a discrete numerical approximation of this equation, we use the trapezoidal rule

$$\sum_{i=1}^{n} c_i \sigma_{i,r} = N_{y_r} \quad (r = 1,2,...,N) \qquad (16)$$

where $\sigma_{i,r}$ = stress value at node i at time t_r, and c_i = coefficients of the trapezoidal numerical integration formula $c_1 = c_n = 1/2$, $c_2 = \cdots = c_{n-1} = 1$ (a higher-order numerical numerical approximation would hardly be helpful because the treatment of boundaries would become complicated, and also because the stress distribution need not be very smooth if fracturing occurs; Fig. 2 bottom).

Fracture Mechanics Aspects and Crack Band Model

The cracking of concrete can be conveniently modeled in a smeared continuum manner but special measures have to be taken

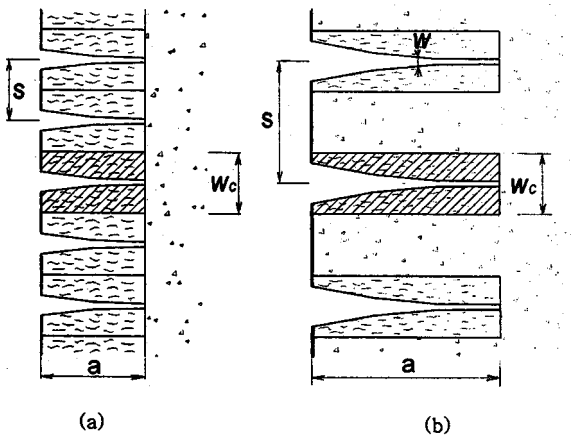

Fig. 3. (a) Parallel thermal cracks at their closest possible spacing given by width of crack band (width of fracture process zone, corresponding to maximum aggregate size); (b) parallel thermal cracks at doubled spacing, with a closed initial crack between each pair.

to satisfy the requirements of fracture mechanics. A simple way to do that is to base the analysis on the crack band model (Bažant 1976, 1982; Bažant and Oh 1983). This model approximately takes into account the localization of distributed cracking into discrete cracks which have a certain characteristic spacing s. Because the adjacent parallel crack bands, simulating parallel cohesive cracks (Fig. 2 middle), cannot overlap (Fig. 3 left), the minimum possible spacing of these cracks must be taken equal to the empirically known width w_c of the crack band. According to the crack band model, the bandwidth w_c must be considered a material property in order to avoid spurious localization of smeared continuum damage with the accompanying spurious mesh sensitivity, and to ensure correct energy dissipation. Roughly $w_c \approx 3d_a$ where d_a = maximum aggregate size.

When the parallel thermal cracks in unreinforced or lightly reinforced concrete become too long, every other crack closes and the spacing of the remaining (dominant) cracks doubles (Fig. 3 right). The doubling becomes repeated whenever the ratio of the length a of the dominant cracks to their spacing s exceeds a certain critical value. This is a phenomenon of bifurcation of equilibrium path, as determined by stability analysis of a system of interacting parallel cracks (Bažant and Ohtsubo 1977; Bažant et al. 1979; Bažant and Wahab 1979, 1980; Bažant and Raftshol 1982; Bažant and Cedolin 1991, Chap. 12). According to linear elastic fracture mechanics, the spacing of the dominant (open) cracks increases roughly as

$$s = \phi a \tag{17}$$

where $\phi \approx 0.69$ (Fig. 3), and as an approximation, we accept this relation for cohesive fracture. The crack spacing, however, cannot be less than about $3d_a$, which corresponds to the effective width of the crack band in the crack band model. Thus the general rule for the dominant crack spacing may be approximately written as

$$s = \psi a, \quad \psi = \max\left(\phi, \frac{3d_a}{a}\right) \tag{18}$$

where ϕ = dimensionless coefficient.

The value $\phi = 0.69$ applies only for unreinforced or weakly reinforced walls. The value of ϕ needs to be reduced if the wall has a load-bearing reinforcement, more precisely, a reinforcement ratio exceeding about 0.2% (which corresponds to the so-called

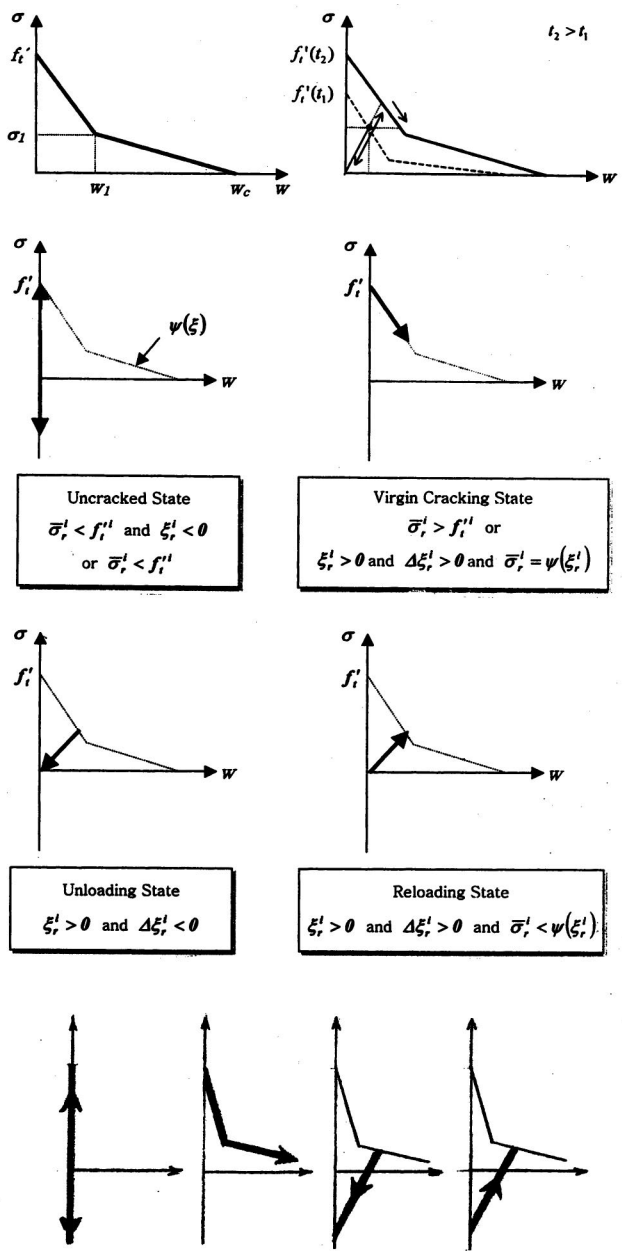

Fig. 4. (Top left) Bilinear softening curve of stress σ versus crack opening displacement w for cohesive crack model assumed for analysis. (Top right) Upward shift of this curve due to strength gain with age. (Middle two rows) Idealized rules for cohesive crack response used in computations—uncracked, virgin cracking (softening), unloading and reloading. (Bottom) Alternative more realistic rules not used in computations.

minimum shrinkage and temperature reinforcement; Bažant and Wahab 1980). If there is a heavy and dense three-dimensional reinforcing mesh, then $s \approx 3d_a$ = constant, for any crack length, which is equivalent to setting $\phi = 0$ in Eq. (18). Since the parallel thermal cracks propagating symmetrically from the opposite faces of the wall cannot be longer than $D/2$, the maximum possible crack spacing in a wall of thickness D is

$$s_{\max} \approx \tfrac{1}{2}\psi D \tag{19}$$

According to the crack band model or the cohesive crack model, the crack-bridging (cohesive) stress $\sigma = f(\delta)$ where $f(\delta)$

=decreasing function of the crack opening δ characterizing the cohesive fracture properties of the material. This function is here assumed as the usual bilinear function defined in Fig. 4 (top).

Since the strains and stresses do not vary monotonically, it is also necessary to define the rules for unloading and reloading of the cohesive crack. An idealized simple rule used in the present computations is shown graphically in Fig. 4 (middle two rows), and an alternative rule not used in computations in Fig. 4 (bottom). These rules are simplified versions of those demonstrated experimentally by Reinhardt and Cornelissen (1984) used in the drying creep studies of Bažant and Chern (1985a, b).

In a general smeared cracking model, one cannot assume the cracking strain to be simply a function of the stress because the dominant crack spacing s may vary. The proper approach is to assume that the smeared cracking strain ξ accumulated over the distance s between the cracks must be equal to the opening width δ of the cohesive cracks, i.e., $s\xi=\delta$ (Fig. 2). In the cohesive crack model, δ is assumed to be a unique decreasing function of the crack-bridging cohesive stress σ, $\delta=f(\sigma)$, which means that

$$\xi_i=\frac{\delta_i}{s}=\frac{f(\sigma_i)}{\max(3d_a,0.69a)} \quad \text{if } \xi_i\geqslant\xi_{i_{\max}} \tag{20}$$

(Fig. 2) where $\xi_{i\,\max}$, introduced to define the loading criterion, represents the maximum tensile cracking strain that has so far occurred at node i (its value must be stored for each node and updated in each time step). Function f may be simplified as a bilinear function beginning its descent at $\sigma=f_t'$ for $\delta=\xi=0$ and terminating at $\sigma=0$ for some critical opening δ_f (Fig. 2).

If the crack opening increases, the increment of cracking strain at node i may thus be written as

$$\Delta\xi_i=C_i\Delta\sigma_i$$
$$C_i=\frac{f(\sigma_i+\Delta\sigma_i)-f(\sigma_i)}{\max(3d_a,0.69a)} \quad \text{if } \Delta\xi_i\geqslant 0, \quad \xi_i\geqslant\xi_{i_{\max}} \tag{21}$$

where C_i=current tangential compliance of cracking at node i, which depends on δ, and thus on ξ.

Since cracks that opened due to hydration heat may later close, one also needs a rule for unloading, and more generally also for reloading and possible renewed virgin loading. A simple rule, which has been used in the present computations, is explained graphically by Fig. 4, and its mathematical formulation is better given later as part of the overall algorithm. A more sophisticated rule for the unloading, not used in the present computations, is defined in the Appendix.

Time Step Algorithm

Substituting Eqs. (14) and (20) for loading or the rules in Fig. 2 or the Appendix for unloading, into Eq. (13), we have the complete incremental stress–strain relation that is needed for step-by-step analysis.

$$\Delta\epsilon_r=(C^i_{v,r}+C^i_r)\Delta\sigma^i_r+\Delta\epsilon^i_{v,r}+\alpha^i\Delta T^i_r \tag{22}$$

in which

$$C^i_{v,r}=J^i_{r+1/2,r+1/2}+\Delta t_r\ \dot{J}^i_{r+1,r+1/2} \tag{23}$$

$$\Delta\epsilon^i_{v,r}=\sum_{q=1}^{r-1}(\sigma^i_{q+1}-\sigma^i_q)\Delta t_r J^i_{r+1,r+1/2} \tag{24}$$

where $C^i_{v,r}$=effective incremental compliance; and $\Delta\epsilon^i_{v,r}$ =effective inelastic strain increment due to viscoelasticity (creep). Both these quantities can be evaluated before solving the variables for t_{r+1}. The step-by-step solution of stresses and strains in time step (t_r,t_{r+1}) may proceed according to the following algorithm (Fig. 3):

1. loop over all nodes $i=1,...,n$.
2. evaluate $C^i_{v,r}$ and $\Delta\epsilon^i_{v,r}$ from Eq. (14). Set $I=1$ (which we call, for the sake uniformity, the first 'iteration,' although, strictly speaking, only $I\geqslant 2$ represent iterations).
3. For the first "iteration," $I=1$, and for all nodes $i=1,...,n$, estimate the average and final stress values in the step as $\overline{\sigma}^i=\sigma^i_r$ and $\hat{\sigma}=\sigma^i_r$.
4. Loop on iterations, $I=1,2,...,N_{it}$.
5. If $\xi^i>0$, go to 10.
6. Now $\xi^i\leqslant 0$. Set $C_i=0$.
7. If $\overline{\sigma}^i<f_t'^i$, go to 15 ($f_t'^i$ is also a function of maturity, i.e., time and temperature; which means f_t' is dependent on time step r and node i.).
8. Now $\overline{\sigma}^i\geqslant f_t'^i$. Set $C^i=\psi(\overline{\sigma}^i)$.
9. Go to 15.
10. If $\Delta\xi^i\leqslant 0$ (crack unloading), go to 14.
11. Now $\xi^i>0$ and $\Delta\xi^i>0$. If $\overline{\sigma}^i<\psi(\overline{\sigma}^i)$, go to 13.
12. Virgin crack loading: Set $C^i=\psi(\overline{\sigma}^i)$ and go to 15.
13. Reloading of crack: Set $C^i=C_u$ where C_u is the specified unloading slope defined by either Fig. 2, or by the Appendix. Go to 15.
14. Unloading of crack: Set $C^i=C_u$.
15. End of the loop on nodes $i=1,...,n$.
16. According to equilibrium condition Eq. (16), calculate

$$\Delta\epsilon=\left[\sum_{i=1}^{n}\frac{c^i}{C^i_{v,r}+C^i_r}(\Delta\epsilon^i_{v,r}+\alpha^i\Delta T^i_r)+\Delta N^i_{y_r}\right]\Big/\sum_{i=1}^{n}\frac{c^i}{C^i_{v,r}+C^i_r} \tag{25}$$

1. For all the nodes $(i=1,...,n)$, calculate

$$\Delta\sigma^i_r=\frac{\Delta\epsilon_r-\Delta\epsilon^i_{v,r}-\alpha^i\Delta T^i_r}{C^i_{v,r}+C^i_r} \tag{26}$$

and set $\overline{\sigma}^i=\sigma^i_r+\frac{1}{2}\Delta\sigma^i_r$, $\hat{\sigma}^i=\sigma^i_r+\Delta\sigma^i_r$.

2. If $I<N_{it}$, or if a specified tolerance is met (which is the end of iteration loop), reset $I\leftarrow I+1$ and go to 5
3. Reset $r\leftarrow r+1$, go to 1, and start the next time step.

Numerical Results

The data on the heat of hydration of concrete are, for convenience, optimally approximated with the function

$$H(t_e)=H_\infty\frac{(t_e-t_0)^n}{a+(t_e-t_0)^n} \tag{27}$$

where H_∞=final heat of hydration (per unit mass of cement); t_0 =delay time for the onset of hydration, and a and n=constants to be determined from experimental data. As seen in Fig. 5 (left), the optimal values of H_∞, t_0, a, and n are 110, 0.15, 1.21, and 0.73 for Type I cement, and 105, 0.2, 1.53, and 0.8 for Type V cement, based on experimental data with $w/c=0.4$ at a constant temperature of 20°C.

To verify function (27) adopted to approximate the hydration heat evolution, an adiabatic temperature rise calculated with this function is compared to the experimental results for concretes made with Type V cement, water/cement ratio 0.40 and coarse aggregate content 989 kg/m^3. Three cases of concrete mixtures are considered, with sand/aggregate ratios 0.42, 0.39 and 0.36 for cases 1, 2, and 3; water contents 160, 181, and 200 kg/m^3, cement contents 400, 450, and 500 kg/m^3, fine aggregate contents 726,

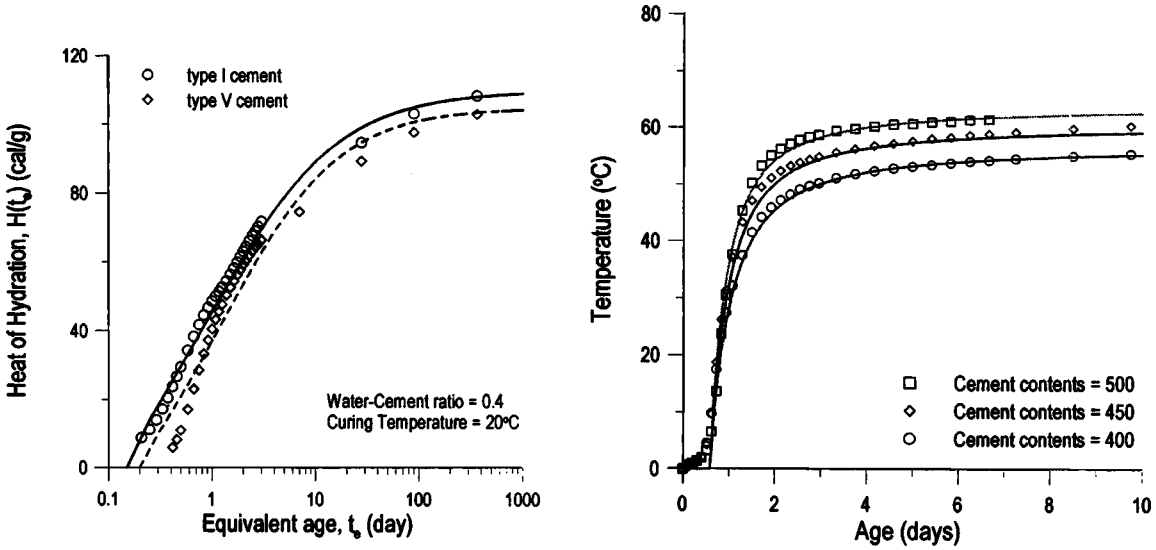

Fig. 5. (Left) Test data on hydration heat generated as function of equivalent age t_e, curve of hydration heat used as input, and results of numerical simulations (because specimens are small enough to neglect their temperature change, heat of hydration is measured under isothermal condition). (Right) Measured curve of adiabatic heating of insulated specimen, and comparison with its numerical simulations for various cement contents (type V).

630, and 544 kg/m^3, and admixture contents 2, 2.26, and 2.5 kg/m^3, respectively. Furthermore, the following data are used in calculations: Cement contents 400, 450, and 500 kg/m^3; activation energy of hydration U given by $U/R=4{,}000$ K (normalized by universal gas constant R); coefficient of heat conductivity 8,790 J/m h °C (2.1 kcal/m h °C); specific heat of concrete 1,170 J/kg °C (0.28 kcal/kg °C), and mass density of concrete 2,320 kg/m^3. As seen in Fig. 5 (right), the results calculated with this function agree well with the experimental data.

Fig. 1 (top) shows two examples of simple structures which are used to verify the present analytical procedure for calculating temperature and crack histories. They are: (1) a wall fixed at ends and (2) a cylindrical (axisymmetric) wall, both 1.2 m thick. For calculating the temperature distributions throughout the concrete wall (Fig. 2 top), a rather fine nodal subdivision (in one dimension) is used (Fig. 2 bottom). The following input data are considered for this example: cement content 300 kg/m^3; concrete temperature at placing 20°C; ambient temperature 20°C, and heat conduction coefficient 9.8 kcal/m^2 h °C.

The calculation of the development of stress distributions and thermal cracking is based on the stress crack–opening displacement curve shown in Fig. 4 (top and middle), in which, according to the CEB-FIP Model Code, $\sigma_1=0.15f_t'$; $w_1=2(G_F/f_t')-0.15w_c$; and $w_c=\alpha_F G_F/f_t'$, where $G_F=k_d(f_c')^{0.7}$, and α_F and k_d are functions of the maximum aggregate size d_a. Further input values: coefficient of thermal expansion$=10^{-5}$/°C, and cylindrical compressive strength of concrete at 28 days$=33.4$ MPa. In the analysis of cracking, the variation of tensile strength with the equivalent hydration period t_e has been considered, expressed as $f_t'(t_e)=0.227[f_t'(t_e)]^{2/3}$ which is the lower-bound estimate of the splitting tensile strength according to the CEB-FIP Model Code (1988), if age t is replaced with t_e. To take into account the increase of tensile strength, the stress–crack opening displacement curve is considered as age dependent, as shown in Fig. 4 (top right).

In the computations, it is assumed, for the sake of simplicity, that the normal force resultants in the cross sections of the wall are zero. This means that the structure is assumed not yet to be prestressed and, if the bottom part of the containment is considered, that the full weight of the containment structure does not yet act in the cross section. To adjust the calculations to any nonzero prescribed normal force in the cross section would of course be easy.

Figs. 6, 7, and 8 show typical computational results. As seen in Fig. 6, the peak temperature is achieved at each node at a time between 1 and 2 days. The overall temperature peak, which occurs in the center of wall, is about 48°C, for the assumptions and input considered here.

Fig. 7 displays the computational results for a cylindrical (axisymmetric) concrete wall. In this case, no cracks develop, which is of course the desired behavior and means that the design is good.

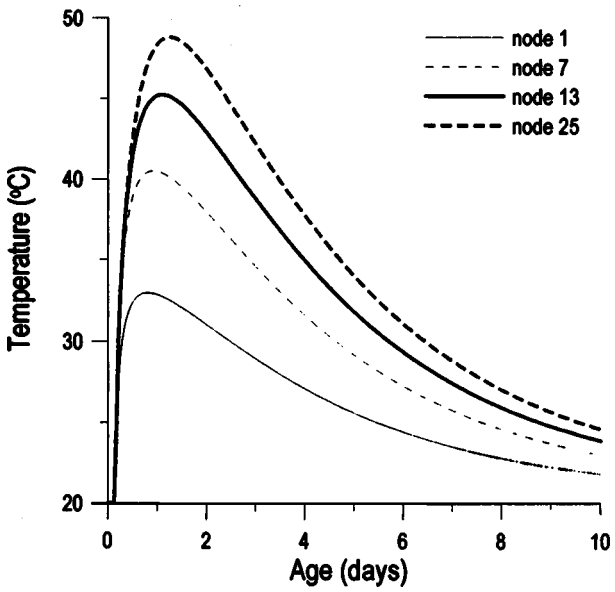

Fig. 6. Calculated histories of temperature at nodes 1, 7, 13, and 25, located, respectively, at distances 0, 15, 30, and 60 cm from surface

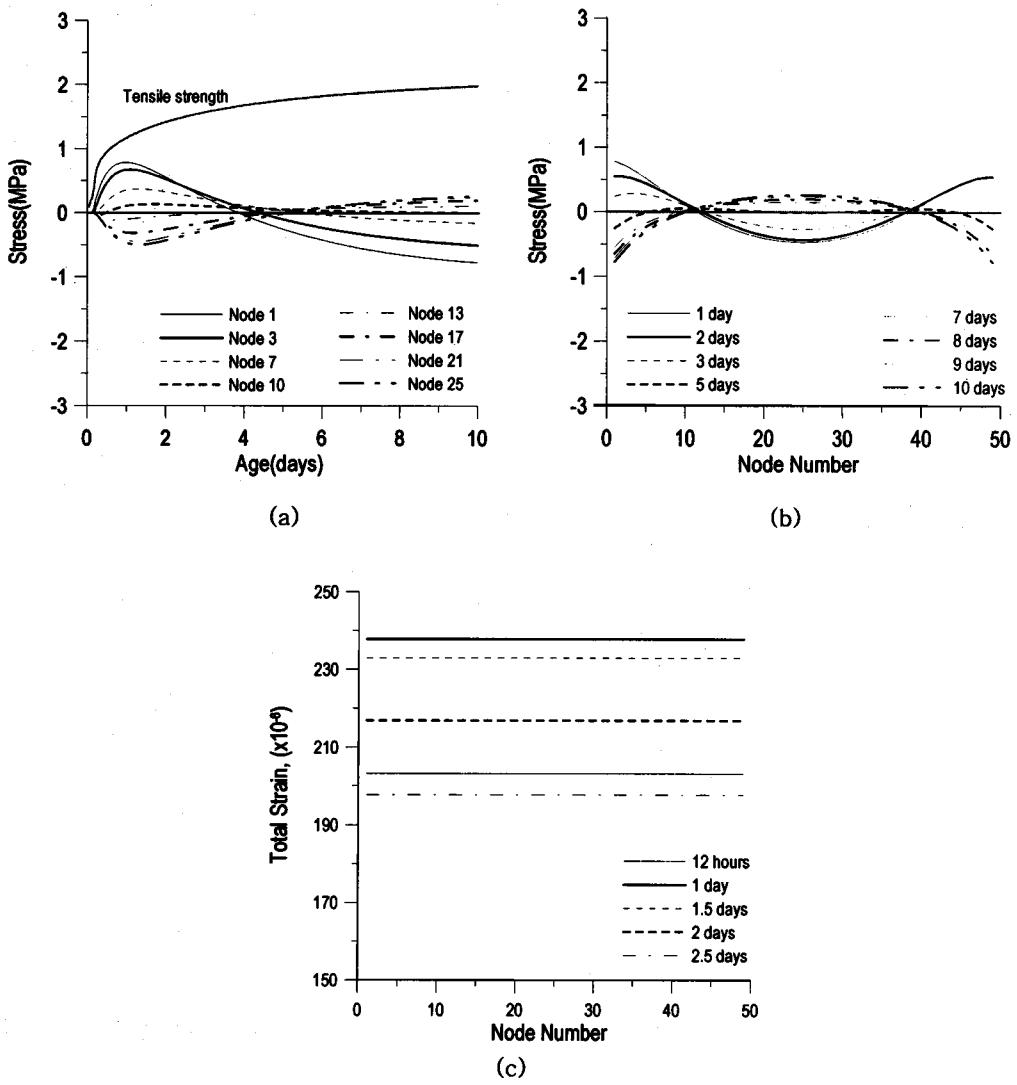

Fig. 7. Numerical results for axisymmetric wall, for which no cracks develop: (a) calculated stress histories at various nodes; (b) stress profiles across wall at various ages of concrete; (c) strain at various ages in longitudinal directions of wall, same for all nodes

To demonstrate the effect of cracking, another computation is made for a concrete wall with fixed boundaries in *y* and *z* directions. In this case, the in-plane normal strains are zero. The results are shown in Fig. 8.

Figs. 7(a and b) and 8(a and b) show that the stress histories undergo a reversal at the time of peak temperature, for the cases both without and with cracking. However, the stress profiles are different. For an axisymmetric wall [Figs. 7(a and b)], the early stress profiles show tension in the surface layer [Fig. 7(b)] but after several days the surface layer goes into compression and a smaller tensile stress develops in the center of the wall. The reason for this behavior is that the early creep is much larger (because of a higher temperature and a lower age) than the late-age creep [this is similar to the development of stress profiles caused by long-time drying (Bažant and Chern 1985a; Bažant and Xi 1994)]. These stress profiles mean that the concrete wall is subjected to internal restraints. For fixed end wall [Figs. 8(a and b)] the early stress profiles show compression through the whole thickness of the wall, but then go into tension, which means that stress evolution in the concrete wall is significantly affected by external restraints. In this case, the stress in the center of the wall is much larger than that at the surface.

The effect of cracking is to reduce the stress levels in general. Fig. 8(c) shows the profile of the cracking strain, which represents the ratio of crack width to spacing. The crack depth is also apparent from this diagram, and the spacing can be back calculated from the crack depth. Fig. 7(c) shows the evolution of the longitudinal thermal strain in the wall. As seen, its maximum is reached in about 1 day.

Conclusions

1. Although the objective of a good design is to avoid cracking, a realistic assessment of the safety of massive concrete walls against damage from hydration heat requires the growth of cracks to be simulated according to the principles of fracture mechanics. The crack band model with smeared cracking, formulated so as to be equivalent to the cohesive crack model, is adopted as an adequate approximation for this purpose.
2. As is well known, the most important characteristic of cracking is the crack opening width, which is determined by the crack spacing. The estimation of crack spacing requires tak-

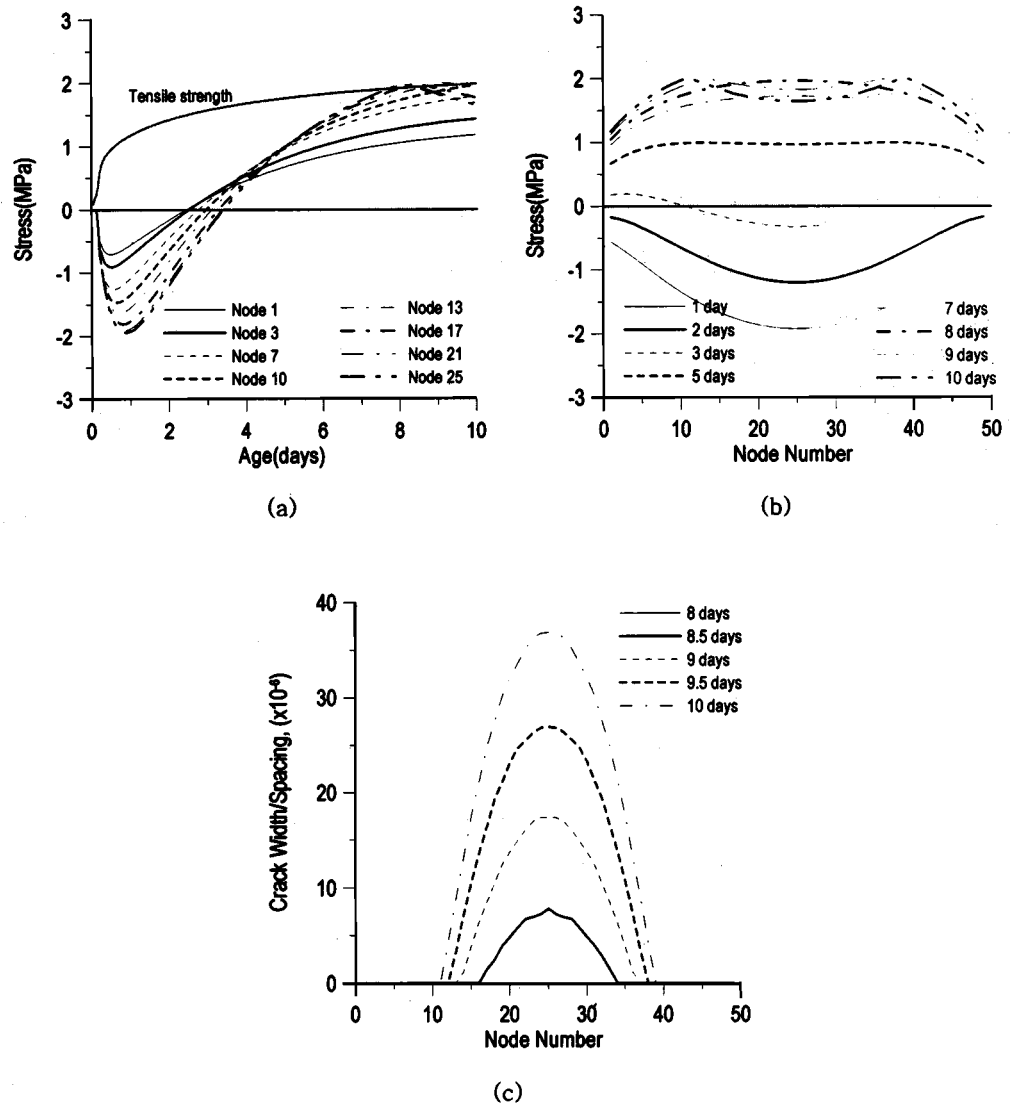

Fig. 8. Numerical results for wall with fixed ends, for which cracks do develop: (a) calculated stress histories at various nodes; (b) stress profiles across wall at various ages of concrete; (c) profiles of cracking strain (crack width divided by spacing) at various times

ing into account what is known about the stability of parallel crack systems. As previous studies showed, the spacing of open cracks increases roughly in proportion to the crack depth unless there is a strong and dense reinforcing mesh.

3. Since the effects of creep and aging are known to be very important, the most realistic model for creep with aging must be used in thermal stress analysis. The advances that have been achieved in this regard are used in developing an up-to-date method of structural creep and fracture analysis and formulating a computational algorithm.

Acknowledgments

Partial funding under Grant No. CMS-9732791 from the U.S. National Science Foundation to Northwestern Univ. is gratefully acknowledged. J.-K. K. wishes to express his thanks for financial support from Korea Institute of Science and Technology, Evaluation and Planing (KISTEP).

Appendix: Alternative Improved Rule for Crack Unloading

A rather simple yet more realistic rule for the unloading behavior of a cohesive crack, which can be used as a replacement for unloading stage (c) in Fig. 3, was formulated (in terms of the cracking strain) and graphically illustrated by Bažant and Chern (1985b). Generalizing this rule slightly by introducing parameter Υ, one may define this rule as follows:

$$\Delta\xi_i = C_i \Delta\sigma_i$$
$$C_i = \Upsilon \frac{g(s\xi_i)}{\xi_i} \quad \text{if } \xi_i < \xi_{i_{\max}} \tag{28}$$

where $\Upsilon \geq 1$ is an empirical parameter, and $\sigma = g(\delta)$ is the inverse function of $\delta = f(\sigma)$ defining the cohesive crack model. In the case that $\Upsilon = 1$, the foregoing rule for unloading means that the tangent of the unloading curve is approximately taken as parallel to the secant of the point on the loading curve of the cohesive crack model that has the same value of δ. In the case where

Υ is taken larger than 1, all the unloading slopes are Υ times steeper than these secants, which causes the unloading curve to shift to the right. Integration of the unloading rule Eq. (28) gives an unloading curve that intersects the displacement axis to the right of the origin and approaches a vertical asymptote lying to the right of the stress axis. These simple features produce unloading curves of an almost realistic shape, resembling the test results of Reinhardt and Cornelissen 1984).

The irreversibility of crack opening at unloading enhances the compressive stress at surface, and thus elevates the tensile stress in the core in the late stage of hydration.

References

Bažant, Z. P. (1976), ''Instability, ductility, and size effect in strain-softening concrete.'' *J. Eng. Mech. Div.*, 102, 331–344; ''Discussion.'' 103, 357–358, 775–777, 104, 501–502.

Bažant, Z. P. (1982). ''Crack band model for fracture of geomaterials.'' *Proc., 4th Int. Conf. on Numerical Methods in Geomechanics*, Univ. of Alberta, Edmonton, Canada, 1137–1152.

Bažant, Z. P. (1995). ''Creep and damage in concrete.'' *Materials Science of Concrete IV*, J. Skalny and S. Mindess, eds., American Ceramic. Society, Westerville, Ohio, 355–389.

Bažant, Z. P. and Baweja, S. (2000). ''Creep and shrinkage prediction model for analysis and design of concrete structures: Model B3.'' *Proc., Adam Neville Symposium: Creep and Shrinkage—Structural Design Effects*, A. Al-Manaseer, ed., American Concrete Institute, Farmington Hills, Mich., 1–83 ⟨http://www.fsv.cvut.cz/kristek⟩.

Bažant, Z. P. and Cedolin, L. (1991). *Stability of structures: elastic, inelastic, fracture and damage theories*, Oxford University Press, New York.

Bažant, Z. P. and Chern, J.-C. (1985a). ''Concrete creep at variable humidity: constitutive law and mechanism.'' *Materials and structures*, Vol. 20, RILEM, Paris, 1–20.

Bažant, Z. P., and Chern, J.-C. (1985b). ''Strain softening with creep and exponential algorithm.'' *J. Eng. Mech.*, 111(3), 391–415.

Bažant, Z. P. and Kaplan, M. F. (1996). *Concrete at high temperatures: material properties and mathematical models*, Longman (Addison-Wesley), London.

Bažant, Z. P. and Najjar, L. J. (1972). ''Nonlinear water diffusion in nonsaturated concrete.'' *Materials and structures*, Vol. 5, RILEM, Paris, 3–20.

Bažant, Z. P. and Oh, B.-H. (1983). ''Crack band theory for fracture of concrete.'' *Materials and structures*, Vol. 16, RILEM, Paris, 155–177.

Bažant, Z. P., and Ohtsubo, H. (1977). ''Stability conditions for propagation of a system of cracks in a brittle solid.'' *Mech. Res. Commun.*, 4(5), 353–366.

Bažant, Z. P., Ohtsubo, R., and Aoh, K. (1979). ''Stability and post-critical growth of a system of cooling and shrinkage cracks.'' *Int. J. Fract.*, 15, 443–456.

Bažant, Z. P., and Planas, J. (1998). *Fracture and size effect on concrete and other quasibrittle materials*, CRC, Boca Raton, Fla.

Bažant, J. P., and Prasannan, S. (1989). ''Solidification theory for concrete creep. I. Formulation,'' *J. Eng. Mech.*, 115(8), 1691–1703.

Bažant, Z. P., and Raftshol, W. J. (1982). ''Effect of cracking in drying and shrinkage specimens.'' *Cem. Concr. Res.*, 12, 209–226; ''Discussion.'' 797–798.

Bažant, Z. P., Şener, S., and Kim, J.-K. (1987). ''Effect of cracking on drying permeability and diffusivity of concrete.'' *ACI Mater. J.*, 84, 351–357.

Bažant, Z. P., and Wahab, A. B. (1979). ''Instability and spacing of cooling or shrinkage cracks.'' *J. Eng. Mech. Div.*, 105(5), 873–889.

Bažant, Z. P., and Wahab, A. B. (1980). ''Stability of parallel cracks in solids reinforced by bars.'' *Int. J. Solids Struct.*, 16, 97–106.

Bažant, Z. P., and Xi, Y. (1994). ''Drying creep of concrete: Constitutive model and new experiments separating its mechanism.'' *Mater. Struct.* 27, RILEM, Paris, 3–14.

Bernander, S., and Gustafsson, S. (1981). ''Temperature stresses in early age concrete due to hydration.'' *Nord Betong, Stockholm*, 2, 25–31 (in Swedish, with English summary).

Bertero, V. V. and Polivka, M. (1972). ''Influence of thermal exposure on mechanical characteristics of concrete.'' *Proc., Int. Seminar on Concrete for Nuclear Reactors*, ACI Special Publication No. 34, Vol. 1., American Concrete Institute, Detroit, 505–531.

Carlson, R. W., and Forbrick, L. R. (1938). ''Correlation of methods for measuring heat of hydration of cement.'' *Ind. Eng. Chem.*, 10, 382–386.

Carslaw, H. S. and Jaeger, J. C. (1959). *Conduction of heat in solids*, 2nd Ed., Oxford University Press, Oxford.

CEB-FIP Model Code. (1988). *Bull. d'Information No. 190a*, Comité Euro-International De Béton, EPFL, Lausanne.

Crank, J. (1957). *Mathematics of Diffusion*, Oxford University Press, Oxford.

Czernin, W. (1962). *Cement chemistry and physics for civil engineers*, Crosby and Lockwood.

Emborg, M. (1985). ''Temperature stresses in massive concrete structures.'' Licentiate thesis, OILL, Luleøa Institute of Technology, Luleøa, Sweden.

Hanson, J. A. (1953). ''A ten-year study of creep properties of concrete.'' *Concrete Laboratory Rep. No. SP-38*, U.S. Dept. of the Interior, Bureau of Reclamation, Denver.

Harboe, E. M. (1958). ''A comparison of the instantaneous and sustained modulus of elasticity of concrete.'' *Concrete Laboratory Rep. No. C-854*, Division of Engineering Laboratories, U.S. Dept. of the Interior, Bureau of Reclamation, Denver.

Jirásek, M., and Bažant, Z. P. (2002). *Inelastic analysis of structures*, Chap. 28 and 29, Wiley, London.

Lea, F. M. (1970). *The chemistry of cement and concrete*, Arnold, London.

Lea, F. M., and Jones, F. R. (1935). ''The rate of hydration of Portland cement and its relations to the rate of development of strength.'' *J. Soc. Chem. Ind. (London)*, 54(10), 63–70T.

Maslov, G. N. (1940). ''Thermal stress states in concrete masses, with account of concrete creep.'' *Izvestia Nauchno-Issledovatel'skogo Instituta Gidrotechniki*, Vol. 28, Gosenergoizdat, Moscow, 28, 175–188 (in Russian).

Neville, A. M. (1981). *Properties of concrete*, Pitman, London.

Reinhardt, H. W., and Cornelissen, H. A. W. (1984). ''Post-peak cyclic behavior of concrete in uniaxial tensile and alternating tensile and compressive loading.'' *Cem. Concr. Res.*, 14(2), 263–270.

RILEM Committee TC 69. (1988). ''State of the art in mathematical modeling of creep and shrinkage of concrete.'' *Mathematical modeling of creep and shrinkage of concrete*, Z. P. Bažant, ed., Wiley, Chichester, 57–215.